RESEARCH ARTICLE

Transitional circulation patterns from full ice cover to ice-off in a seasonally ice-covered lake

Katie Stagl Hughes[1,2,3] · Alexander L. Forrest[1,2] · Alicia Cortés[1,2] · Fabián A. Bombardelli[1,2]

Abstract

There is consensus that under-ice circulation presents multiple phases through the winter, and that different mechanisms dominate each period. In this work, measurements of temperature, water velocity, conductivity, and dissolved oxygen from Lake Massawippi, Quebec, Canada, obtained during the ice-covered season in 2019, were used to characterize the time scales of different winter regimes and transitions among dominating circulation mechanisms. Lake circulation during this period began with a single-cell convection induced by sediment flux pulses in early winter. The single-cell convection decayed into a brief quiescent period. Radiatively driven convection then formed a convectively mixed layer in late winter. The defined mixed layer and temperature structure provided the necessary conditions for the formation of a potential rotational feature, which briefly formed immediately prior to ice break-up. Ice break-up led to complex hydrodynamics that persisted for nearly 28 days following full ice-off. Dissolved oxygen was directly correlated with the varying circulation features throughout the field campaign. This work provides a quantitative measure to delineate the transitions between under-ice regimes and provides novel insights into the subsequent circulation during and after ice break-up.

Keywords Winter limnology · Under-ice gyre · Under-ice measurements · Under-ice circulation · Ice-off mixing dynamics · Lake Massawippi

Introduction

The drivers of circulation patterns (both horizontal and vertical) in seasonally ice-covered lakes shift throughout the entire ice-on. The dominant drivers of circulation have been characterized as sediment fluxes immediately after ice-on (Likens and Ragotzkie 1965) during the period referred to as *Winter I*, and radiatively driven convection in the later stages of winter (Farmer 1975) referred to as *Winter II*, with wind and inflows having additional impacts on circulation (Bengtsson 1996; Kirillin et al.

2012). During the initial onset of ice cover, the water column develops inverse stratification, with 0 °C water at the ice-water interface and the warmest, denser water at the sediment–water interface, close to the temperature of maximum density in freshwater (T_{MD} ~4 °C) (Kirillin et al. 2012). *Winter I* is dominated by the strong initial release of heat stored in the sediments of ~3–5 W/m^2 immediately after ice-on (Likens and Ragotzkie 1965; Malm 1998) and then tapering off down to 0.5 W/m^2 through the winter season (Zdorovennova 2009). Bathymetric features and the attenuation of solar radiation in the water column contribute to temporal and spatial variability in sediment fluxes, which can induce baroclinic motion and/or advection of heat to the deeper parts of the lake via density currents (Zdorovennova 2009; Ramón et al. 2021). *Winter II* is thought to occur once heat fluxes from sediments stabilize, and the snow cover permits solar radiation to penetrate through the ice. As near-surface water below T_{MD} warms, increasing density will induce instabilities initiating radiatively driven convection (RDC) right underneath the ice; this can erode the density structure formed over the winter (Farmer 1975). Observations of RDC have

✉ Katie Stagl Hughes
    kestagl@ucdavis.edu

1   Department of Civil and Environmental Engineering, University of California, Davis, One Shields Ave., Davis, CA 95616, USA

2   Tahoe Environmental Research Center, University of California, Davis, 291 Country Club Dr., Incline Village, NV 89451, USA

3   Shiley School of Engineering, University of Portland, 5000 N Willamette Blvd, Portland, OR 97203, USA

provided evidence of a distinct four-layer stratification structure consisting of a surface layer (SL), convectively mixed layer (CML), entrainment layer (EL), and quiescent layer (QL) (Mironov et al. 2002; Forrest et al. 2008). The resulting penetrative convection drives a deepening and warming of the CML (Austin 2019; Yang 2021; Bouffard et al. 2016; Farmer 1975; Jonas et al. 2003). Both RDC and sediment fluxes have the potential to induce density currents, internal waves, horizontal transport, and gyre formation (Bouffard et al. 2016; Farmer 1975; Huttula et al. 2010; J. Malm et al. 1997; Rizk et al. 2014; Ulloa et al. 2019; Vehmaa and Salonen 2009).

Gyres are defined in this work as rotational features influenced by the Coriolis force that are not constrained by the shoreline and are non-dispersive (e.g., Kelvin and Poincaré waves; Bouffard and Boegman 2012). In addition, gyres exhibit a dome-like isothermal structure (Forrest et al. 2008). Gyres are commonly found in large open-water lakes (Beletsky et al. 1999; Beletsky 1996; Kerfoot et al. 2008) and recent research in winter limnology has identified the presence of gyres in mid-size, ice-covered lakes. Gyres in mid-size, ice-covered lakes have been observed through satellite imagery, field measurements, and three-dimensional modeling (Huttula et al. 2010; Forrest et al. 2013; Kirillin et al. 2015; Kouraev et al. 2019, 2016; Salonen et al. 2014; Steel et al. 2015). The radius of under-ice gyres is typically on the scale of the internal Rossby radius of deformation, $\Lambda = \frac{c}{f} = \frac{\sqrt{g' H_e}}{f}$, where $g' = g \Delta\rho / \rho_0$ is the reduced gravity to account for the change in density in the water column, f is the Coriolis frequency (Kundu et al. 2016) and $H_e = h_1 h_2 / (h_1 + h_2)$ is the equivalent depth for a two-layer stratified system. For open water, h_1 would be the depth of the epilimnion and h_2 would be the hypolimnion, while the ice-on period would typically consider the convectively mixed layer as h_1 and the quiescent layer as h_2 (Bouffard and Boegman 2012). Gyres under ice are now known to exist from temperate to polar regions and to drive lateral transport under the ice during a time commonly thought to be quiescent (i.e., not driven by winds); however, the mechanisms of formation, maintenance, and decay remain poorly understood, and represent a unique balance of the conditions that are known to vary annually (Salonen et al. 2014). The direction of the rotation of lake gyres under-ice has varied across the literature (Ramón et al. 2021). Both cyclonic and anticyclonic gyres have been observed in the northern hemisphere using field instrumentation and hydrodynamic modeling (Huttula et al. 2010; Forrest et al. 2013). The initiating mechanisms have been hypothesized to include sediment fluxes, RDC, differential snowmelt runoff, and moat formation (Huttula et al. 2010; Kirillin et al. 2015; Ulloa et al. 2019). Further field campaigns are needed to resolve the thermal structure at appropriate horizontal length scales and to aid in predicting where these transient phenomena exist from year to year.

Another poorly studied area of winter limnology is the circulation patterns that exist during the transition phases from open water to ice-on and ice-off to open water. The consensus in the literature is that ice-on initiates sediment flux (Kirillin et al. 2012), and after ice-off, the water column is highly susceptible to wind-induced mixing and under-ice stratification, driving either partially or fully mixed water column as a result of the interplay between both (Cortés and MacIntyre 2020). Heat fluxes and wind are likely the dominant forcing mechanisms for circulation during this period. However, the time scales of circulation, water velocities, and impacts on water quality during the transitional periods are not well understood.

The duration, circulation patterns, transition phases of each winter regime, and mixing at ice break-up are important to consider due to the varying physical mechanisms that hinder or promote the redistribution of nutrients, nonmotile organisms, and/or pollutants. This paper presents the results of high-frequency temperature, conductivity, dissolved oxygen, and velocity measurements in a mid-latitude, seasonally ice-covered lake in the winter of 2019 from after freeze-up to immediately after ice break-up. The distinct periods of *Winter I,* the transition from *Winter I to II* (herein referred to as *Deep Winter*), and *Winter II,* were delineated by assessing the heat flux between near-surface and near-bottom temperature sensors. The results from the field campaign are used to address the evolution of circulation during ice-on and the transition period of ice-off, which includes temperature structure, circulation patterns, potential gyre formation, and full mixing events.

Methods

Site description

Lake Massawippi, located in Southern Quebec, Canada, is an elongated, mid-size (14 km long by 1.6 km wide, maximum depth of 86 m, average depth of 41.6 m, surface area equal to 18.7 km^2, volume equal to 0.75 km^3), mid-latitude (45.25 °N, 71 °W) lake with a consistent seasonal ice cover (typically from January to April). Lake Massawippi is classified as a dimictic lake due to seasonal periods of overturn in both spring and fall.

Lake Massawippi has similar characteristics to other lakes that have been documented to exhibit under-ice circulation patterns driven by Coriolis forcing, which include minimal snow cover to allow penetrative solar radiation, and minimal inflows that allow formed circulation patterns to persist after forcing has ceased (Forrest et al. 2013; Rizk et al. 2014).

The primary inflow to the lake is the Tomifobia River in the southern part of the lake. The outflow is the Massawippi River at the northern sub-basin, which has a small dam one kilometer downstream from the outlet (Fig. 1A). The maximum annual water level fluctuation is 1.5 m, with an average water level fluctuation of 0.6 m (Government of Quebec).

Field measurements

In January 2019, three in-situ, subsurface moorings (top floats located at 2 m below the water surface to avoid contact with the ice) were deployed to capture water temperature, specific conductance, dissolved oxygen, and water velocities in the northern end of the lake (~1000 m width). The moorings were deployed through the ice-on day of the year (day) 31 (31-Jan-2019) and serviced in May following ice-off, day 114 (24-Apr-2019). One mooring was deployed at 26 m depth, approximately 100 m from the eastern shoreline. Two moorings were deployed mid-lake in the pelagic region (~46 m), approximately 300 m NW from the eastern mooring. The mooring transect line was approximately perpendicular to the shoreline (Fig. 1).

In addition, a series of conductivity, temperature, and depth (CTD) profiles were conducted using an RBR Concerto, with a sampling frequency of one second. The six profiles were measured across the transect line of the moorings (east to west) on 29-Jan-2019 (star in Fig. 1B). Holes were drilled through the ice to lower the instrument through the water column.

A meteorological station was mounted on top of the roof of a building, approximately 100 m from the northeastern shoreline of the lake and roughly 12 m high (Fig. 1B), which included two temperature and relative humidity probes, shortwave radiation sensor, and an anemometer, with a sampling rate of 10 min. Table 1 provides a summary of the mooring configurations and depths of each sensor, and the meteorological station, including the resolution and accuracy of each instrument used. For all data presented in the figures, temperature records from the thermistors and CT cells were interpolated to 10-min averages, and the meteorological and dissolved oxygen data were processed using hourly averages. The beam correlation of the four beams from the acoustic Doppler current profiler (ADCP) was assessed for quality assurance of the data. All four beams demonstrated a 90% correlation factor for the duration of the field deployment, with a correlation factor of 70% or greater signifying acceptable data. The downward-facing ADCP recorded one-meter cell size and resolved 39 m of the water column. The sampling ensemble used 60 pings at a ping interval of two minutes, and time between ensembles was 20 min. The data were post-processed using hourly bin averages. Although the specifications of the RDI Teledyne Sentinel V ADCP state the resolution of the instrument is 0.1 cm/s, bin size, and sampling frequency selected in this study yielded that accuracy of the velocity magnitude values was below 1 cm/s. Velocity magnitudes less than 1 cm/s are still shown in this paper to demonstrate flow structures and patterns.

Satellite imagery was obtained from the NASA Earth Observinσg System Data and Information System (EOS-DIS) Worldview to determine and confirm the approximate dates of ice-on, partial ice, and full ice cover conditions of
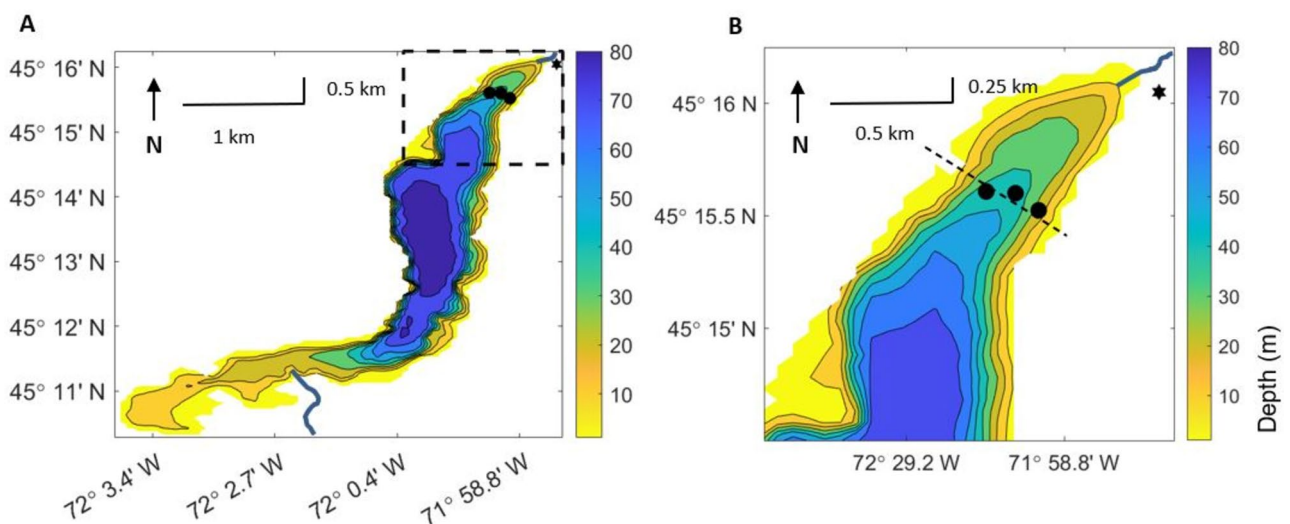
Fig. 1 a Lake Massawippi bathymetry with dashed line indicating study site. The Tomifobia River inlet is at the SE shoreline, with the outlet at the northern end of the lake. **B** Lake Massawippi bathymetry map of northern sub-basin with location of measurements. Circles: temperature chain mooring locations, square: ADCP mooring location, star: meteorological station. Black dashed line is the transect line for CTD casts. The Tomifobia River outlet is at the northern end of the lake

**Table 1** Mooring setup and field equipment specifications

Station	Instrument	Depths (m)	Parameter	Sampling Rate	Accuracy	Resolution
Mid-Lake Mooring	2 RBR Duo³ CT cells	5.5, 43	Conductivity	2 sec	±0.003 mS/cm	0.001 mS/cm
			Temperature		±0.002 ºC	<0.00005 ºC
	10 RBR Solo Thermistors	5.5, 6, 7, 9, 10, 18, 26, 36, 40, 42	Temperature	1 - 30 sec	±0.002 ºC	<0.00005 ºC
	1 miniDOT	43.5	Dissolved Oxygen	10 min	±0.3 mg/L	0.01 mg/L
Mid-Lake ADCP Mooring	Teledyne RDI Sentinel V: downward-facing	1 m cell size 39 m resolved	Current speed/direction	• 60 pings • 2 min ping intervals • 20 min between ensembles	±0.3 cm/s	0.1 cm/s
Near-shore Mooring	6 RBR Solo Thermistors	5.5, 14, 22, 23.5, 24.5, 25	Temperature	5 - 30 sec	±0.002 ºC	<0.00005 ºC
Met Station	CS Temperature - EE181	-	Temperature	10 min	±0.2 °C	-
		-	Relative Humidity	10 min	±(1.4+0.01*RH)	-
	CS Wind Monitor-HD	-	Wind Speed	10 min	±0.3 m/s	0.1666 m/s
		-	Wind Direction	10 min	±3°	-
	CS Pyranometer - 301	-	Shortwave	10 min	±5% for daily total radiation	-

the lake. NASA Worldview provides daily temporal resolution and a spatial resolution of 250 m.

Ice-covered results

Initial conditions

Ice began forming on the lake on 26-Dec-2018 (via site inspection), and there was partial ice cover at the deepest part of the lake, the geographical midpoint until 17-Jan-2019 (day 17; via satellite imagery). The instruments were deployed through the ice, therefore the mean temperature at the start of winter is unknown. At the time of deployment, 31-Jan-2019 (day 31), ice thickness was measured at the drilled holes for the CTD profiles, and it varied between 23 and 46 cm, with the thickest ice toward the edge of the lake. The six CTD profiles are shown in Fig. 2 along the mooring transect line, which were roughly 50 m apart. The profiles depicted are separated by a +0.5 °C offset. The CTD profiles indicate that inverse stratification had fully developed with 0 °C near the ice-water interface, and a sharp temperature gradient at ~3 m. The initial water temperature from the nearshore mooring at 5 m and 25 m was 1.6 °C and 2.6 °C, respectively. The water temperatures from the pelagic mooring at 5 m and 40 m was 1.8 °C and 3.1 °C, respectively
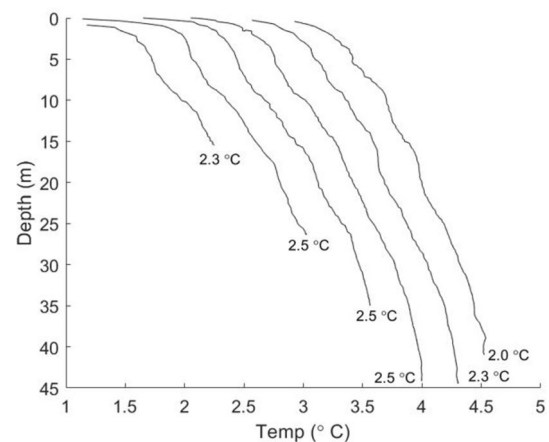
Fig. 2 Six CTD casts on Jan. 29, 2019, across the lake along the mooring transect line with a +0.5° C offset

(Fig. 3). The initial temperatures of deployment indicate that Lake Massawippi would be classified as cryostratified because the water column was not isothermal and closer to 0 °C (Yang 2021). The vertical temperature structure of the water column was homogenous across the lake but varied ±0.25 °C at the same depths (Fig. 2).
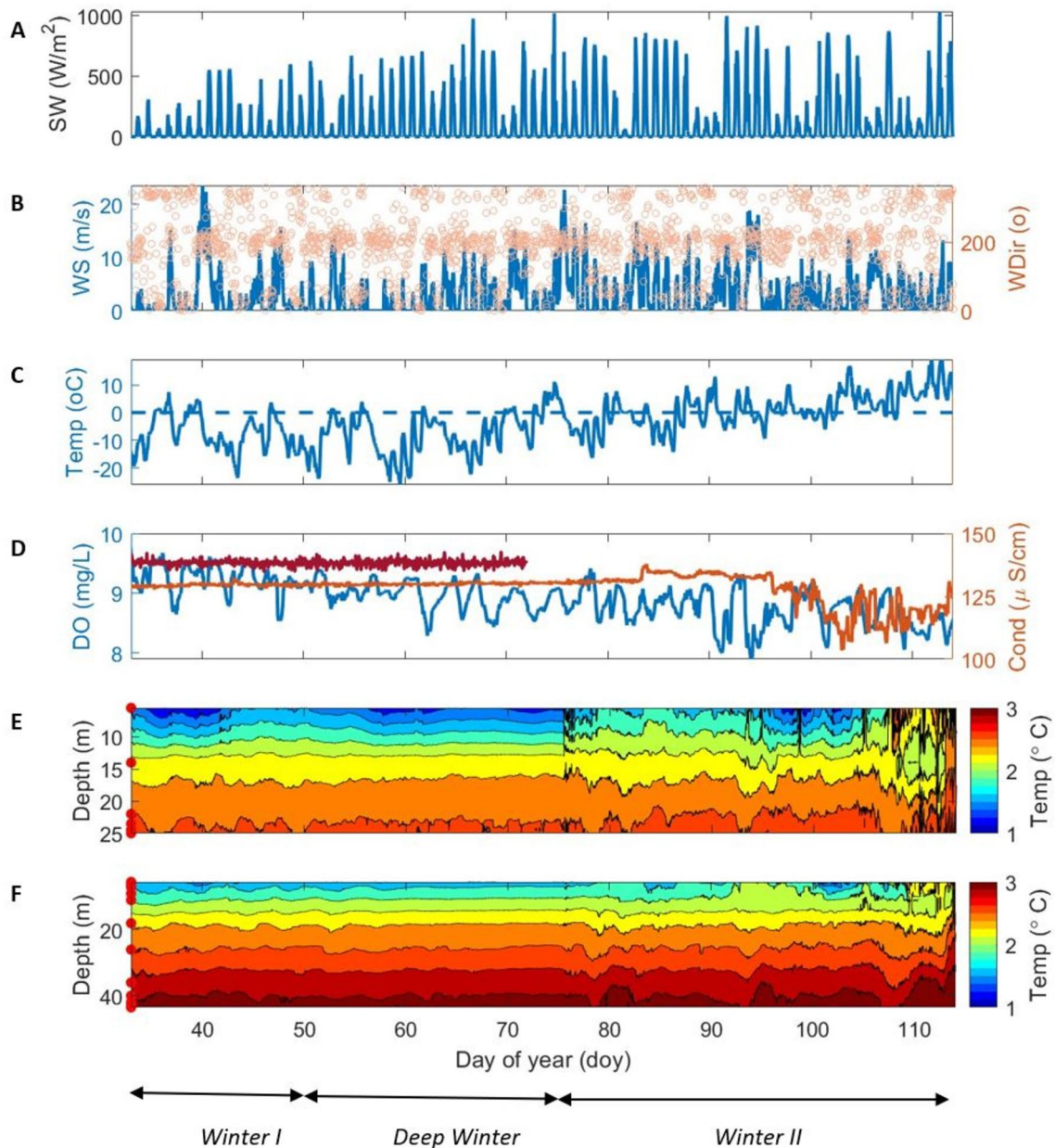
Fig. 3 *Ice-on*. Meteorological and water temperature data from thermistor chains for the ice-on period (day 31–114). The red circles on the y-axis on panels **E**, **F** indicate the thermistor locations. Meteorological conditions of **A** shortwave radiation (SW), **B** wind speed (WS) and direction (WDir), **C** air temperature (Temp), **D** dissolved oxygen (DO; blue), near-surface conductivity (Cond; orange) and bottom conductivity (maroon), and water temperature (°C) contours averaged at 10 min from the **E** nearshore and **F** mid-lake thermistor chains

During the winter, the dominant wind direction was W-SW, with gusts up to 24 m/s. Ice-off occurred on 24-Apr-2019 (day 114; personal communication by local resident N. LeBaron and confirmed by satellite imagery). Due to consistent cloud cover in satellite imagery during the onset of spring ice break-up, it is possible that partial ice cover conditions were present before day 114.

In Fig. 3, the meteorological conditions and temperature of the water column at the nearshore and mid-lake sites from the start of deployment through the ice-on period (day 31–114) are shown. The delineation of winter regimes (*Winter I, Deep Winter,* and *Winter II*) at the bottom of Fig. 3 was determined through the methods presented in this paper.

Physical mixing—temperature and water velocity

The transitional periods between *Winter I*, *Deep Winter*, and *Winter II* were determined by calculating the heat flux through the water column, $W = \rho c_p K_z \frac{\partial T}{\partial z}$, where ρ is the density of the water, c_p is the specific heat of water, K_z is the eddy diffusivity, and $z = 0$ at the water surface. For an inversely stratified water column, the temperature gradient, $\partial T / \partial z$, is the difference between the deeper thermistor and the shallower thermistor at any given location on the thermistor chain. The eddy diffusivity was calculated using a one-dimensional approximation of the heat balance equation, $\frac{\partial T}{\partial t} = \frac{\partial}{\partial z} K_z \frac{\partial T}{\partial z}$. A first-order approximation of the derivative for temperature was used for the thermistors on each mooring line. Derivatives were averaged over the time period where the daily change in temperature was greater than 0.01 °C (from day 31 to 50) to finally estimate a mean K_z of 0.1 cm^2/s that was applied to the ice-covered period. This value agrees with the expected eddy diffusivity found in lakes of similar size as our study site (Bengtsson 1996). The heat flux equation assumes a one-dimensional vertical transfer of heat from the bottom up and neglects advection. During the ice-covered period and inverse stratification, a stable and unstable water column is indicated by a positive and negative heat flux, respectively.

In Fig. 4: *Winter I*, the meteorological conditions, surface, and bottom heat fluxes, nearshore and mid-lake thermistor chains, horizontal magnitudes, vertical velocities, and direction of flow from day 33 to 75 are provided. The estimated heat flux between the bottom two thermistors (depth 42 and 43 m) reached a maximum value of 3 W/m^2 on day 35 and then continued at ~1 W/m^2 until day 58. Near-surface heat flux values were estimated to be significantly greater from day 33 to 44 (maximum values of 16 W/m^2 at day 39). The heat flux at the surface thermistors declined to zero on day 44 followed by a constant heat flux of 5 W/m^2 until day 75. Velocity measurements show that from day 38 to 44 there was a layer of horizontal flow of 2 cm/s that extended from 5 to 12 m, and pulses of upward vertical flow of 1 cm/s that extended through the full water column. During periods of upward flow, the horizontal direction of the flow was an onshore current of ~290° (W-NW), perpendicular to the western shoreline. When the upward pulses of flow relaxed, the flow switched direction by 180°, with the direction of flow at ~110° (E-SE) flowing offshore toward the deeper part of the lake (Fig. 4).

The surface waters on day 32 were ~1.65 °C. The culmination of low shortwave radiation, negative air temperatures and minimal wind speeds permitted further ice accumulation and the thickening of the cool surface layer to temperatures of 1.15–1.3 °C by day 39. The accumulation of cold water was disrupted by a sustained wind event of 24 m/s from day 39 to 41, followed by a 10 m/s wind event on day 42. The surface water temperature increased during the wind events from 1.15 to 1.57 °C at the nearshore mooring and 1.31 to 1.73 °C at the mid-lake mooring. The increase in temperature was likely caused by a displacement of the cooler surface waters by barotropic oscillations of the ice sheet (Bengtsson 1996). Once the wind event relaxed the water temperatures returned to temperatures observed on day 32, ~1.65 °C.

The isotherms became predominantly quiescent and there was little thermal variation from day 50 to 75 (Fig. 3). There was less structure and directionality of the flow below 12 m and the pulsing pattern as previously observed was no longer present, which coupled with the heat fluxes of 0–5 W/m^2, signified the end of *Winter I* on day 50.

On day 75 there was a sustained wind event of 22 m/s that caused an increase in temperature at 5 m of 0.2 °C at the mid-lake site and 0.5 °C at the nearshore site (Fig. 5). From day 75 to 98, the water column experienced alternating stable and unstable temperature gradients in the surface waters, contributing to heating and cooling, and development of a mixed layer. Penetrative solar radiation induced heating of the surface layer, which caused the isotherms to rise from day 75 to 78, with a vertical upward flow of 1 cm/s and diurnal pulses of horizontal flow of 1.5 cm/s with a consistent directionality of 250° (W-SW). Then, the surface waters demonstrated periods of cooling and heating with heterogeneity between the mid-lake and nearshore sites. A cooled layer was present from day 81 to 84 and 86 to 105 at the nearshore site; conversely, the cold layer was only present from day 84 to 86 at the mid-lake site. There was no identifiable structure to the flow from day 81 to 86. In addition, the vertical temperature structure began to deviate from the inverse stratification observed at the beginning of deployment (Fig. 6). The middle of the lake demonstrated a vertically mixed layer of 2 °C extending to 9 m on day 80, then cooled to 1.76 °C and decreased in depth to 7 m on day 84.

The circulation pattern observed from day 75 to 78 was repeated from day 86 to 98. Increased effects of shortwave radiation, air temperatures above 0 °C, and a sustained wind event of 10 m/s from the west resulted in a rejuvenated mixed layer on day 92 at the mid-lake site to a depth of ~11 m (Fig. 5). From day 98 to 104, the stratification was rapidly alternating between thermally stable and unstable. It is important to note that the heat flux equation is one-dimensional and does not account for advection of heat due to the movement of the water. During this time, atmospheric cooling once again created a cool surface layer from day 100 to 105.

There was a sustained wind event from day 105 to 107 of 5 m/s with a consistent W-SW direction. On day 107, the
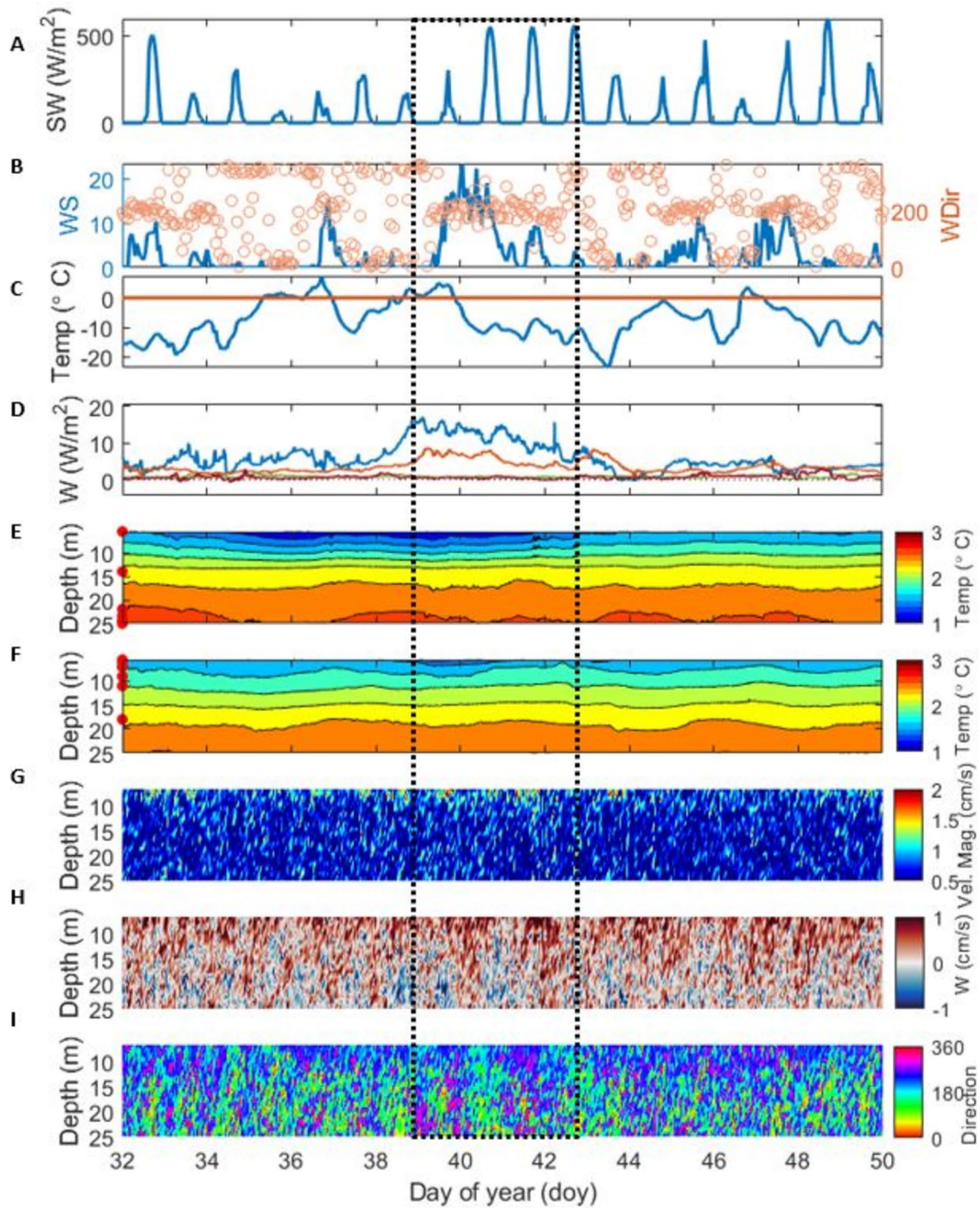
Fig. 4 *Winter I*. The red circles on the y-axis on panel **D**, **E** indicate the thermistor locations. Meteorological conditions of **A** shortwave radiation, **B** wind speed and direction, **C** air temperature, **D** heat fluxes from 43 to 42 m thermistor (red), 42 to 40 m thermistor (green), 7 m to 6 m thermistor (orange), 6 to 5.5 m thermistor (blue), and water temperature (°C) contours averaged at 10 min from the **E** mid-lake thermistor chain and **F** nearshore thermistor chain. Hourly averages from the ADCP including **G** horizontal velocity magnitude values, **H** vertical velocities, and **I** direction of flow from day 33 to 50. Note: there is less reliability in velocity magnitudes below 1 cm/s
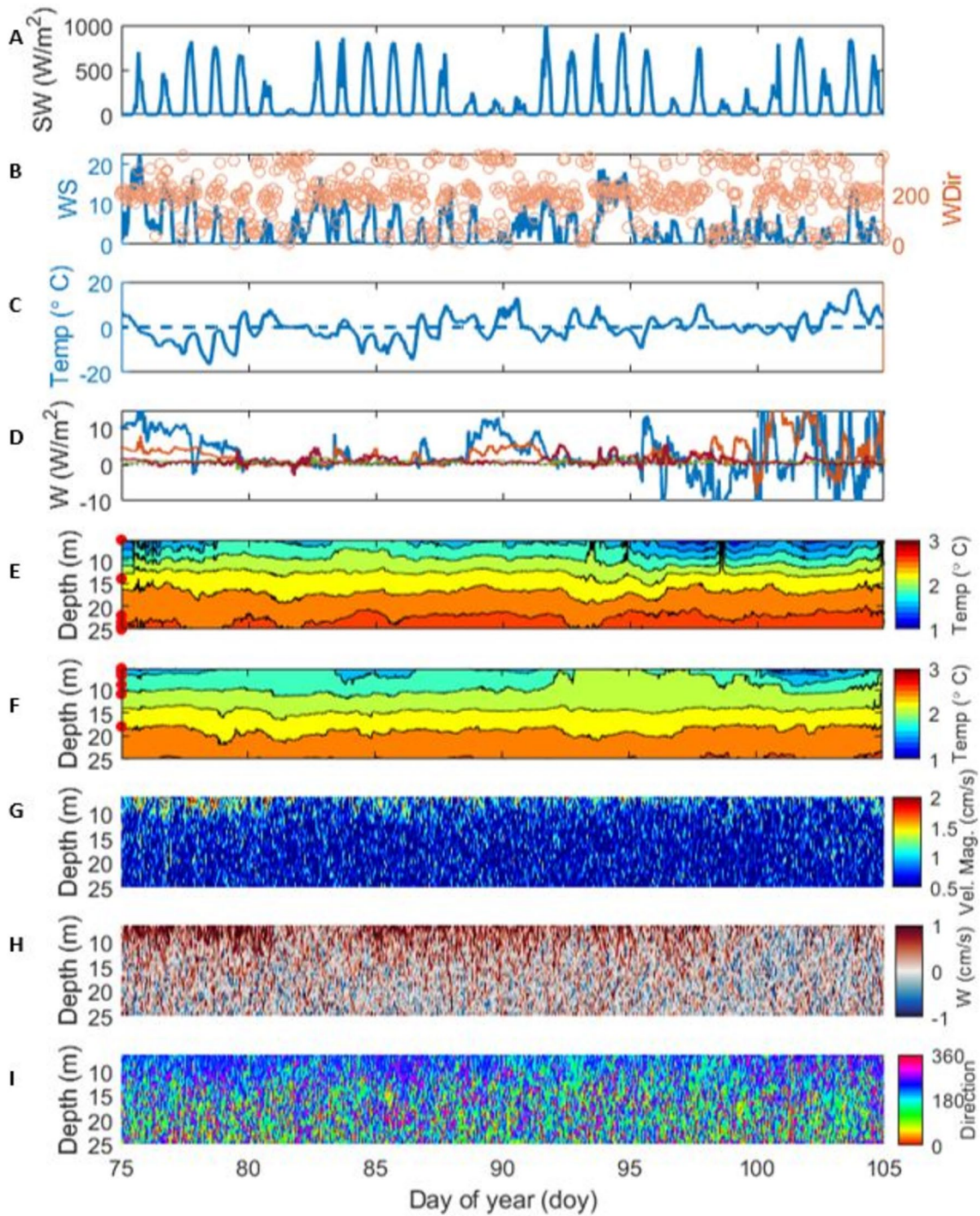
Fig. 5 *Winter II*. Same caption as Fig. 4 except depth of temperature structure and water velocities are limited to 25 m

Fig. 6 A Vertical temperature profiles from mid-lake thermistor chain at 12:00 pm EST in increments of 6 days from day 78 to 96. **B** Vertical temperature profiles shown in (**A**) between 5 and 15 m
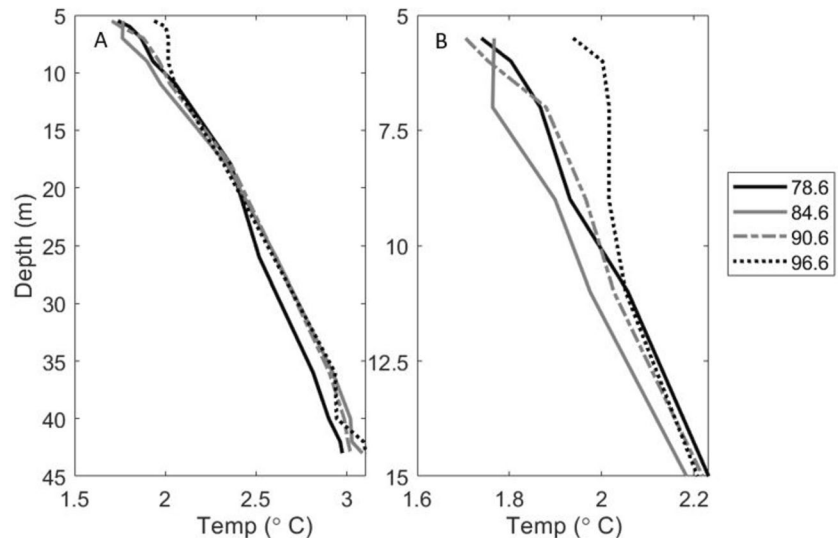
temperature structure presented a density instability at the surface followed by a cold-water mass of 2 °C expressed at a depth of 15 m at the nearshore site with surrounding water of 2.3 °C. The flow structure once again indicated horizontal and vertical flow confined to the surface mixed layer, 5–15 m. From day 105 to 110, the northward water velocities increased to 0.5 cm/s, followed by increased vertical velocities of 0.5 cm/s from day 105 to 112. There were no appreciable eastern velocities during this time. A cold-water mass was expressed at the mid-lake thermistor chain 3.5 days later at 15 m with the same temperature structure as the nearshore site from day 110 to 113. The cold-water mass and increased velocities in the mixed layer were dominated by the tumultuous transition from ice-on to open water (Fig. 7). The air temperature during the day from day 105 onward was above zero, which would signify that there could have been open water at another location in the lake, but this cannot be confirmed by satellite imagery due to significant cloud cover.

Tracers—conductivity and dissolved oxygen

Conductivity was measured at the mid-lake site at 5.5- and 43.5-m depth (~2.5 m above bottom). The sensor located near the bottom stopped recording after day 71 while the top sensor recorded for the full-time period (Fig. 3D). The average conductivity measured near the bottom (43.5 m) from day 31 to 71 was 138.4 µS/cm while the conductivity near the surface (5.5 m) was 129.7 4 µS/cm. There was a steady increase in conductivity near the surface of 0.054 µS/cm/day from day 31 to 83 near the surface likely due to salt exclusion from the ice.

On day 83, conductivity values started changing rapidly with an immediate increase in the near-surface sensor of

6.75 µS/cm in six hours followed by a steady decline in conductivity of −0.35 µS/cm/day from day 83 to 96. The initial increase in conductivity coincides with a 10 m/s S-SW wind event. The pycnocline was likely above the near-surface CT cell (5.5 m) and steadily accumulated salts at a rate of 0.094 µS/cm until the wind event initiated an instability in the surface layer stratification. In addition, increased RDC could have eroded the temperature stratification near the surface, contributing to a density distribution susceptible to instabilities. From day 93 to 94, there was an 18 m/s S-SW wind event with a delayed response of the conductivity on day 96 of a decrease by 7.88 µS/cm in 8 h. The conductivity continued to demonstrate rapid, large fluctuations with the most dramatic shifts occurring from day 103 to 108 at ±18.9 µS/cm in 4 h with the meteorological conditions having a direct influence on the observed fluctuations.

Dissolved oxygen was measured at the bottom of the mid-lake site with a sampling interval of 10 min. Hourly averages of dissolved oxygen are shown in Fig. 3D. At the beginning of the field experiment dissolved oxygen was initially measured to be 9.31 mg/L. Average daily fluctuations of dissolved oxygen under ice were ±0.75 mg/L. The fluctuations in dissolved oxygen are aligned with the measured air temperature, with daily extrema occurring at the same time until day 53, shown in Figs. 3C, D.

A spectral analysis (Bendat and Piersol 1986) was applied to the dissolved oxygen data. From day 53 to 105, the dissolved oxygen demonstrated a cyclic fluctuation with a return period every 93 h (Fig. 8). Maximum fluctuations under ice occurred from day 90 to 114 with values of ±1.32 mg/L. The depletion rate of dissolved oxygen for the duration of the ice-on season was −0.01 mg/L/day, but the DO content at the bottom of the lake remained above 8 mg/L for the duration of ice-on, which is higher than expected for
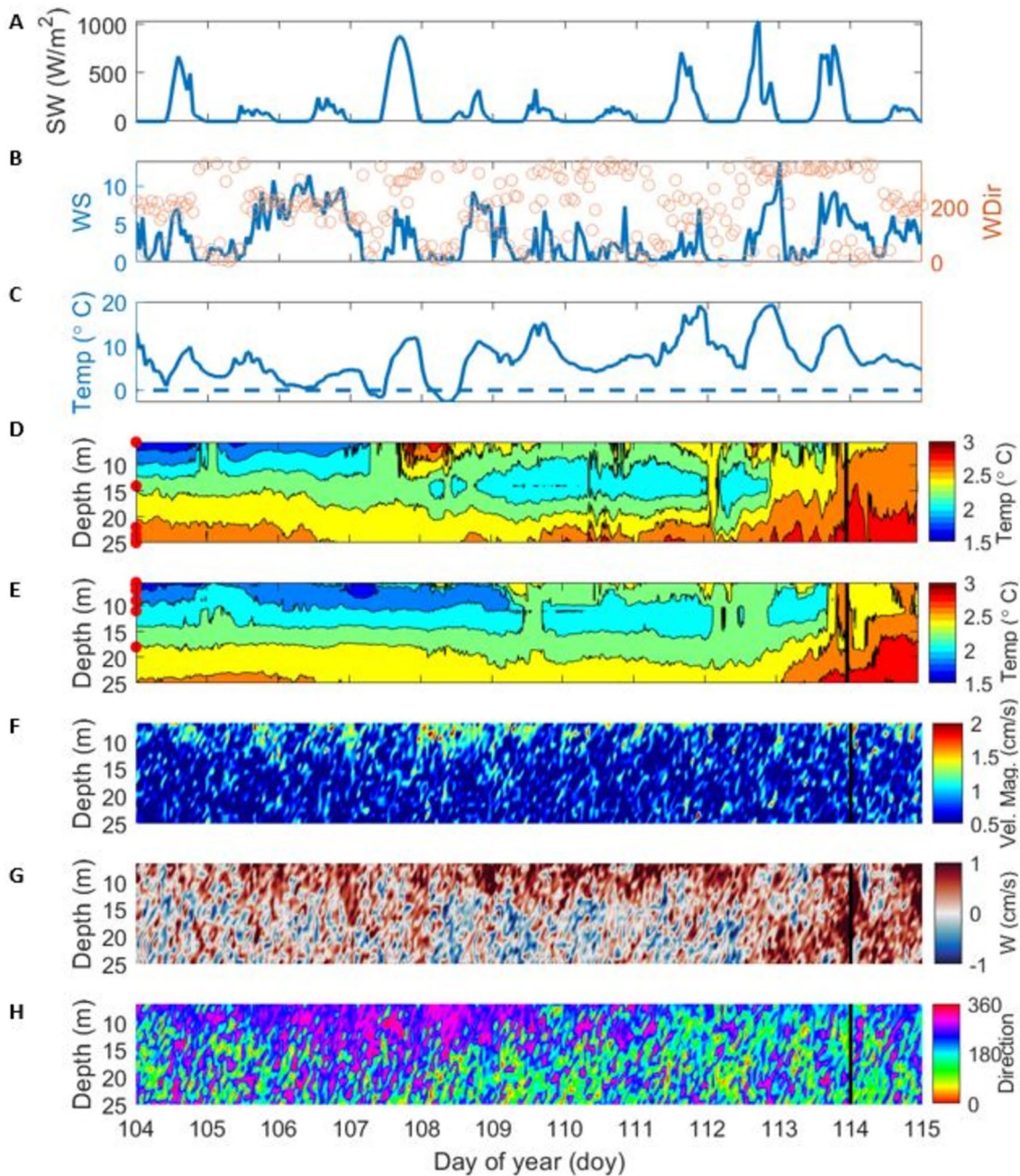
Fig. 7 *Potential rotational feature formation.* The red circles on the y-axis on panel D-E indicate the thermistor locations. Meteorological conditions of **A** shortwave radiation, **B** wind speed and direction, **C** air temperature, and water temperature (°C) contours averaged at 10 min from the **D** mid-lake thermistor chain and **E** nearshore thermistor chain. Hourly measurements from the ADCP include **F** horizontal velocity magnitude values, **G** vertical velocities, and **H** direction of flow from day 104 to 116. Ice-off occurred on day 114, denoted by the thick black line

ice-covered lakes. Typically, ice-covered lakes experience hypoxia by the end of the winter season (Perga et al. 2023; Yang et al. 2020).

Ice-off results

Physical mixing—temperature and water velocity

The meteorological conditions prior to ice-off consisted of several days of air temperatures above freezing and wind
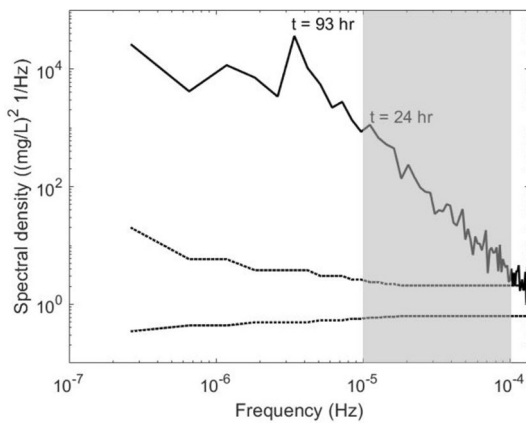
Fig. 8 Spectral analysis of hourly averaged dissolved oxygen from day 53 to 105. 95% confidence intervals are indicated with dashed lines. The inertial subrange expands from 10^{-5} to 10^{-4} Hz, shaded gray

events of 6–9 m/s from the NE. Complete ice-off conditions in the study area occurred on day 114. Immediately after ice-off, the water column remained inversely stratified with a top/bottom temperature difference of 0.6 °C (2.5 °C near the surface at 5.5 m and 3.1 °C at the bottom, 43 m) and spatial homogeneity across the lake. The water column remained below the T_{MD} for 12 days after ice-off.

Prior to ice-off (day 112), the currents were dominated by vertical migration of the bottom waters to the surface with small velocities (0.1 cm/s), which coincided with a southeastern wind event of 9 m/s. When the wind ceased (day 113.5–114.5), the vertical flow was then confined as a band of flow from 15 to 25 m. As the lake became ice-free, this vertical flow continued, but the magnitude decreased. On day 115 the vertical upward flow evolved into a flow separation followed by a horizontal layer of flow in the surface waters. The vertical velocities exhibited a small upward flow (0.1 cm/s) from 5 to 18 m and small downward flows (−0.1 cm/s) from 18 m to the bottom over 8 h (Fig. 9). On day 115, the horizontal flow was confined to the upper layers of 5–10 m; the north velocities shifted from 0.1 to −1.3 cm/s instantaneously with horizontal magnitudes of 0.2 cm/s at 170 °(S). The flow direction was parallel to the shoreline and away from the outlet.

On day 117, the water column became unstably stratified and the temperature structure of the water column exhibited spatial heterogeneity between the nearshore and interior regions. A cold-water layer of 2.7 °C extended from 9 to 35 m surrounded by 2.9 °C at the mid-lake site. In addition, there was a change in direction at both the surface and bottom waters. At 33 m, the flow conditions switched from southern-directed flow with downward vertical velocities to northern flow with upward vertical velocities. Conversely, the surface waters reversed flow from upward to downward

velocities. The cold-water mass continued to express as an 18-m layer that oscillated between ascent and descent in the bottom waters from day 117 to 130. From day 117 to 122, measurements of vertical velocities indicated a flow separation with periods of upward and downward velocities of ±1 cm/s. From day 118 to 121, the downward velocities were confined from 18 m to the bottom of the lake with pulses of upward flow above 18 m. The flow structure reverses on day 122 with upward velocities confined from 31 m to the bottom and downward velocities in the overlying waters.

The nearshore site continued to warm with periods of full mixing (day 117–120, 123–126, and 131) and unstable stratification (day 120–123, 126–131, 132–137, 139–142). During the calm meteorological conditions, there was continued heating of the surface waters until an increase in air temperatures to nearly 20 °C, which was followed by a full mixing event at the nearshore site and partial mixing at the mid-lake site on day 127. A sharp transition of the vertical direction of flow at the mid-lake site during the partial mixing event (e.g., deepening of warmer (~5.7 °C) surface waters) occurred.

The water column warmed instantaneously at both sites on day 130 during a sustained southwesterly wind event of 8 m/s. The horizontal flow increased at the surface and the bottom with speeds of 2 cm/s, and pulses of upward and downward flow. The direction of the flow was alternating 180 degrees between the north and south for the duration of the mixing event.

An additional full mixing event at the nearshore site occurred from day 130.5 to 132, due to constant air temperature and a sustained southwest wind event with an average wind speed of 9 m/s. This mixing event was observed at the mid-lake site on day 131 with less severity or abruptness. These mixing events were followed by weak stratification, expansion, and warming of the hypolimnion. The hypolimnetic waters rose to the surface until constant warming established a stronger stratification, keeping the hypolimnetic waters from rising again. From day 132 onward, stable stratification occurred in the surface layers from 5.5 to 18 m. The T_{MD} isotherm migrated between 20 and 40 m, with underlying bottom waters operating below the T_{MD} (unstable thermal stratification). The CT cell was no longer recording during this period, but the bottom waters could be stably stratified provided a larger salt content. The bottom waters continued to operate below the T_{MD}, while the surface waters continued to warm for the duration of the field measurements (Fig. 10).

Tracers—conductivity and dissolved oxygen

The conductivity at the time of ice-off was 130.97 μS/cm then decreased to a minimum of 118.94 μS/cm on day 116. The surface waters continued to accumulate salts at a linear
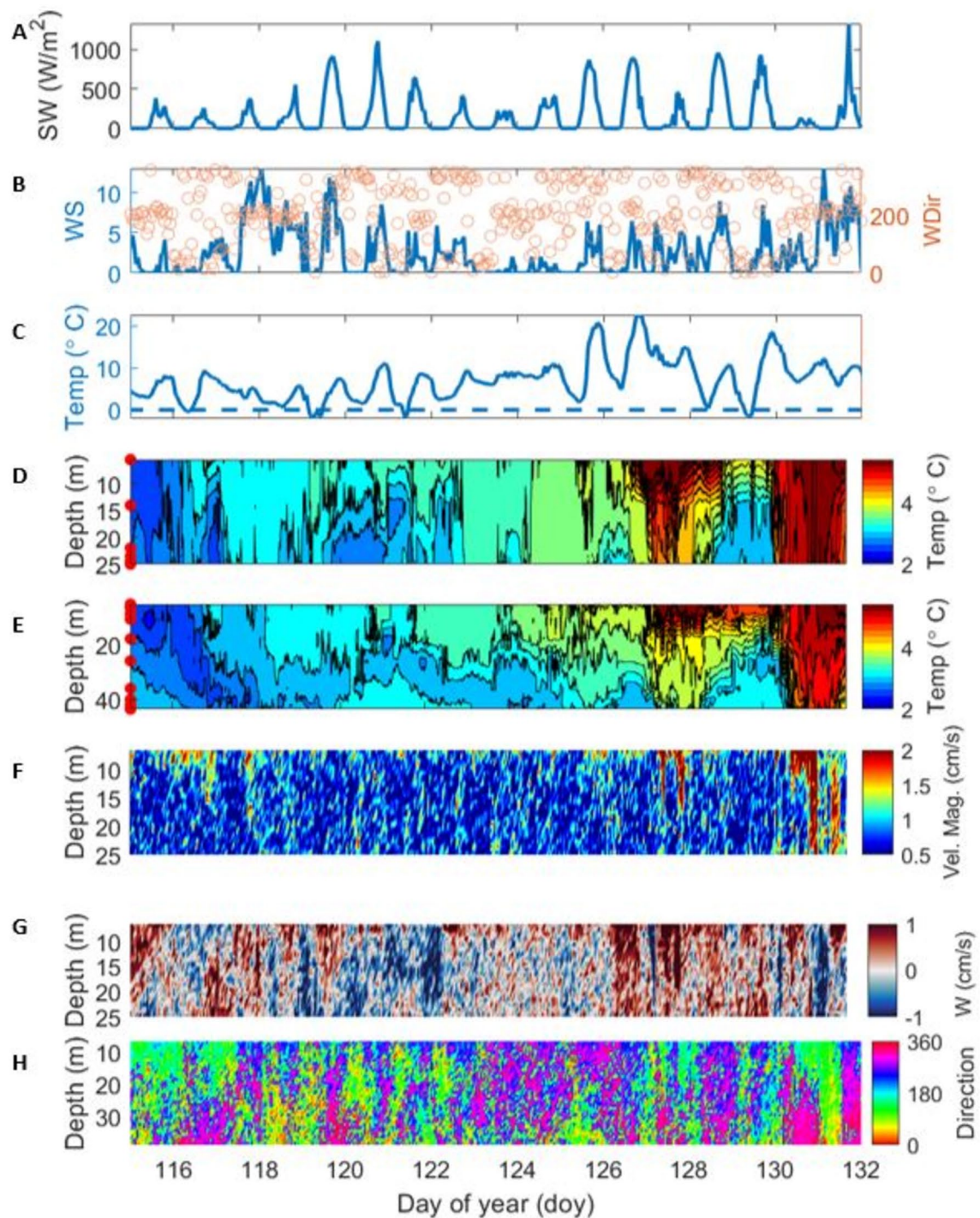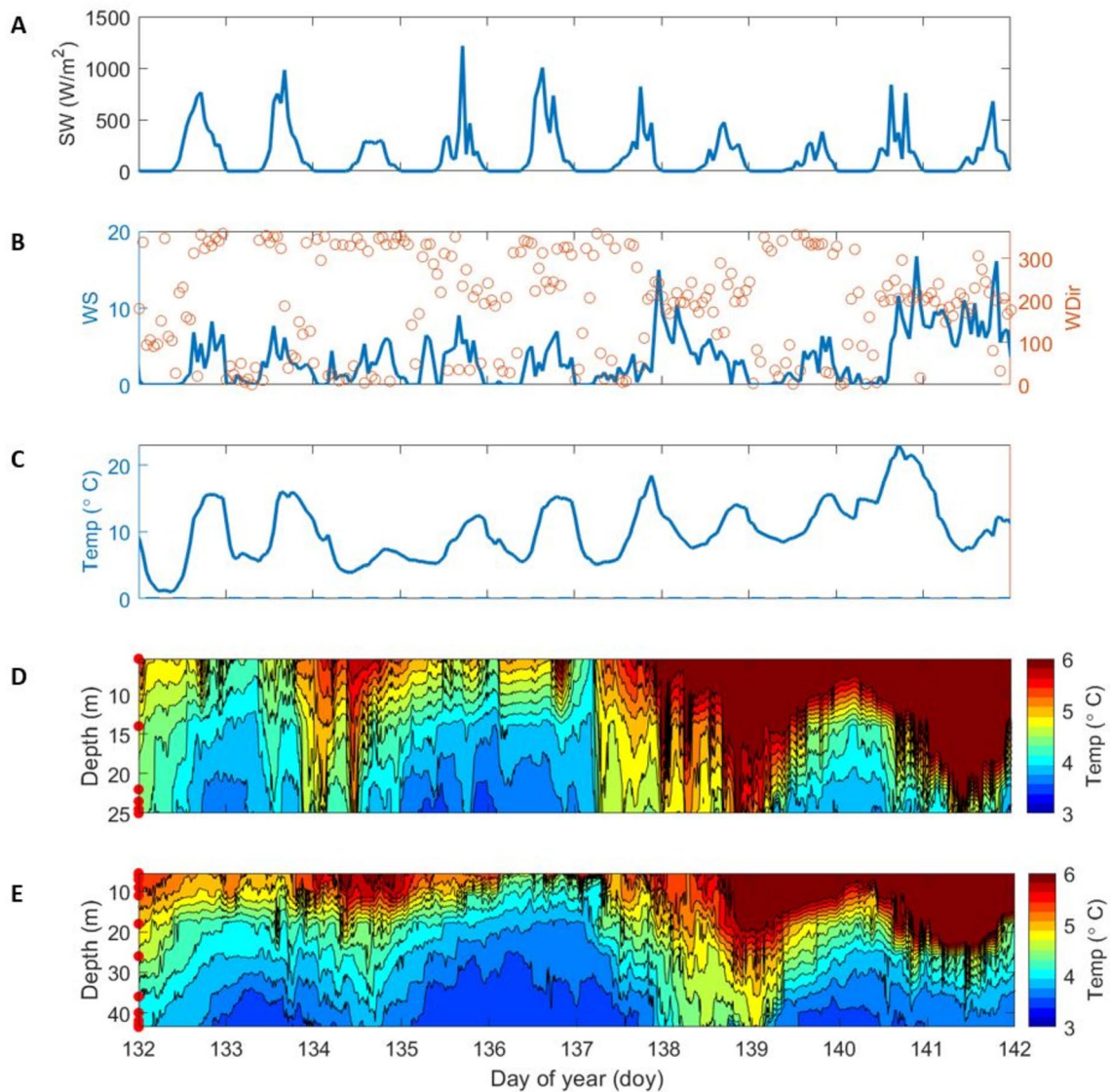
Fig. 9 *Following ice-off*. The red circles on the y-axis on panel **D**, **E** indicate the thermistor locations. Meteorological conditions of **A** shortwave radiation, **B** wind speed and direction, **C** air temperature, and water temperature (°C) contours averaged at 10 min from the **D** mid-lake thermistor chain and **E** nearshore thermistor chain. Hourly measurements from the ADCP include **F** horizontal velocity magnitude values, **G** vertical velocities, and **H** direction of flow from day 115 to 132

rate of 1.24 μS/cm/day, with occasional daily fluctuations of ±12.6 μS/cm. The conductivity and dissolved oxygen measurements after ice-off are shown in Fig. 8.

The dissolved oxygen at the time of ice-off was 8.5 mg/L and four days after ice-off, day 118, increased to a maximum of 10.8 mg/L, but dropped to 8.7 mg/L in five hours. This sharp decline coincides with the downward mixing event

Fig. 10 *Open water*. The red circles on the y-axis on panel D-E indicate the thermistor locations. Meteorological conditions of **A** short-wave radiation, **B** wind speed and direction, **C** air temperature, and water temperature (°C) contours averaged at 10 min from the **D** mid-lake thermistor chain and **E** nearshore thermistor chain. From day 132 to 142

from 118 to 120. From day 119 to 120 the dissolved oxygen experienced another sharp fluctuation of ±2.2 mg/L, which is when the vertical direction of flow rapidly changed directions. Then the dissolved oxygen steadily increased from 7.95 mg/L on day 120 to 10.23 mg/L on day 126, again coinciding with the change in the vertical flow structure of the water column. On day 126 the DO decreased from 10 mg/L to 8.6 mg/L and remained at that value for one day until increasing back to 10 mg/L on day 128 when the cold-water mass was migrating vertically upward. The most severe fluctuation occurred on day 128–130, with fluctuations of ±2.6 mg/L of DO, when there is clear evidence of a vertical and horizontal shear flow (Fig. 9).

Discussion

Winter I and *Winter II* are widely accepted ice-covered regimes that have been reviewed in the literature (Kirillin et al. 2012); however, the transition points and durations of each regime have not been strictly specified. Results from the work included in this study are used to propose a new method to delineate the end of *Winter I* and the start of *Winter II*, and to characterize the period between these two that we called *Deep Winter*. *Deep Winter* is characterized by minimal fluctuations of temperature throughout the water column, and indistinct flow structure with near zero water velocities. The heat fluxes between the bottom thermistors and near surface thermistors were used to determine the

stability of stratification and identified distinct regimes during the ice-cover period. Large heat fluxes between the near-surface thermistors (> 5 W/m^2) at the beginning stages of ice-on indicated the development of stratification due to ice growth, and bottom heat fluxes ranging from 2 to 5 W/m^2, as stated by Likens and Ragotzkie (1965), are the proposed signifiers of *Winter I*. It is proposed that *Deep Winter* begins when the average daily fluctuations of heat fluxes in the surface and bottom waters are within 0–5 W/m^2 for a consecutive amount of time (for Lake Massawippi ~5 days). *Deep Winter* ends when the first observation of a negative heat flux in the surface thermistors occurs, marking the beginning of *Winter II*. A negative heat flux indicates a thermal instability, which could be attributed to horizontal advection, RDC, or the accumulation and plunging of saline meltwater. As *Winter II* progresses, the surface heat fluxes exhibit high variability (e.g., positive and negative heat fluxes within the same day, and hourly changes greater than 10 W/m^2).

The circulation patterns associated with each of the *Winter I*, *Deep Winter*, *Winter II*, and *ice-off* time regimes are reviewed and discussed for Lake Massawippi. Figure 10 provides a schematic of the governing circulation patterns for each winter regime.

Table 2 provides a summary of the explicit documentation of the time scales for *Winter I*, a transition phase (*Deep Winter*), and *Winter II* for ice-covered lakes.

Lakes Sunapee, Simcoe, and Massawippi experienced similar durations for *Winter II*. Perga et al. (2023) indicated that *Winter I* was the dominant winter regime, but this is limited to high-altitude lakes with extensive snow cover. Buffalo Pound Lake is significantly shallower, which would contribute to the longer effects of sediment heat flux that were observed. In addition, Perga et al. (2023) the formation of ice cover and a decline in dissolved oxygen as the signifier for *Winter I*. The transition to *Winter II* occurred when the dissolved oxygen increased. This method would not have delineated the winter regimes in Lake Massawippi, as the oxygen remained above 8 mg/L for the duration of the ice-covered season. Bruesewitz et al. (2015) used the rate of change in mean daily stability as an indicator of transitions between the three winter regimes with a threshold of three standard deviations. Stability outside the threshold was used to indicate *Winter I* and *Winter II*, but there were few data points outside that threshold to distinctly differentiate *Deep Winter* from *Winter II*. Yang et al. (2020) used the development of inverse stratification as the initiation of *Winter I* and the presence of nonzero Thorpe displacements as the initiation of *Winter II*. A transitory period was not presented for this study. The influence of sediment heat flux was shortest for Lake Simcoe, which could be attributed to its vast surface area.

Winter I regime

The progression of ice growth established inverse stratification with steady heat fluxes from the bottom from day 31 to 44, suggesting simultaneous stabilizing forces from the surface and bottom of the lake, and is the proposed period of *Winter I*. At the lakebed, sediment flux and salt accumulation are bottom-up stabilizing forces. While brine rejection resulting from ice growth at the surface is destabilizing, the associated negative heat flux dominates and results in the dominant stabilizing force of the water column at the surface. The temperature gradient at the surface increased during this period, which potentially supports salt accumulation near the ice-water interface (Olsthoorn et al. 2022). This was then maintained by the gradual accumulation of salt seen in the conductivity record near the surface of 0.054 µS/cm/day while, at the bottom of the lake, conductivity increased at a slightly faster rate of 0.06 µS/cm/day due to respiration processes occurring at the sediments (MacIntyre et al. 2018). In addition, wind remained a source of circulation as wind events coincided with sudden temperature changes in the water column on day 44. Wind has the potential to induce ice sheet oscillations, which would result in a barotropic internal wave (Bengtsson 1996).

From the ADCP record, the currents during *Winter I* (day 31–44) demonstrated pulses of upward flow (~1 cm/s), extending through the whole water column, coupled with a surface layer of flow perpendicular to the shoreline (270°), flowing from shoreline to the pelagic region. The flow perpendicular to the shoreline is the result of the conservation of mass from the upward pulses of flow induced by sediment heat and solutes fluxes. In addition, the dissolved oxygen measurements exhibited pulsing increases with daily fluctuations of ±1.5 mg/L during upward flow conditions (Fig. 3D).

Table 2 Time scales of winter regimes for ice-covered lakes

Lake name	Surface area (km^2)	Mean depth (m)	Winter I (days)	Deep Winter (days)	Winter II (days)	References
Sunapee	16.5	10	39	76	24	Bruesewitz et al. (2015)
Buffalo Pound	29.5	3.8	80–110	–	30	Cavaliere and Baulch (2020)
Simcoe	722	15	10–19	–	38–42	Yang et al. (2020)
Massawippi	18.7	41.6	~50	31	39	

This observed pulsing in the dataset suggests an intermittent circulation pattern potentially being driven by diurnal weather fluctuations (Bruesewitz et al. 2015). The proposed circulation pattern for this period is a single-cell convection initiated by sediment heat and solutes fluxes, and conservation of mass (MacIntyre et al. 2018; Kirillin et al. 2012; Malm 1998; Rahm 1985), but this process was dampened by the continuation of ice growth sharpening the temperature gradient at the surface.

The theorized values of vertical velocities by Malm (1998) were estimated by momentum, heat transfer, continuity, and thermal equations of state equations, and yielded values that ranged between 10^{-3} and 10^{-5} m/s. The reference frame for the derivations assumed a sloping bottom and heat flux as the only driving mechanisms for horizontal flow. By continuity, the downslope current resulted in upward vertical velocities at the deepest part of the lake. The configuration of the mid-lake, downward-looking, subsurface ADCP mooring did not capture the theoretical return flow at the ice-water interface nor the descending density current, which by continuity, must be present. Figure 10A provides a conceptual sketch of the circulation patterns during this time. The weakening of the temperature gradient at the surface in the heat fluxes

coincides with the pulses of flow (Fig. 4D), which signifies that the influence of the flow creates a more mixed layer at the surface.

The results of sediment fluxes in Lake Massawippi indicate that in deep lakes, (deep defined by light being attenuated before reaching the bottom of the lake) *Winter I* could be much shorter of a time period (e.g., on the time scale of weeks versus months). In addition, it is important to consider the interactions of ice growth/brine rejection and sediment fluxes, as these mechanisms are working in tandem to alter circulation under ice. The circulation patterns established by sediment fluxes and ice growth set up the initial conditions for the ice-covered time period, with a dampening effect of those circulation patterns as the lake progresses through *Deep Winter*.

Deep Winter regime

On day 41, there was a sustained wind event which was likely translated to the water through ice sheet oscillations, increased mixing near the surface, and a corresponding decrease in the temperature gradient at the ice-water interface (Bengtsson 1996). The stabilizing forces reached an equilibrium point after the wind event and the pulses of

Fig. 11 Schematic of mooring locations (black rectangle shows the ADCP mooring) and circulation patterns during *Winter I*, *Deep Winter*, and *Winter II*: **A** single-cell convection in *Winter I*, **B** stabilized forces of ice growth and sediment flux in *Deep Winter*, **C** establishment of the convectively mixed layer shown with the dashed line, increased central upwelling at the center of the northern sub-basin with decaying vertical flow away from the center in *Winter II*. The direction of horizontal flow is shown with the yellow arrow
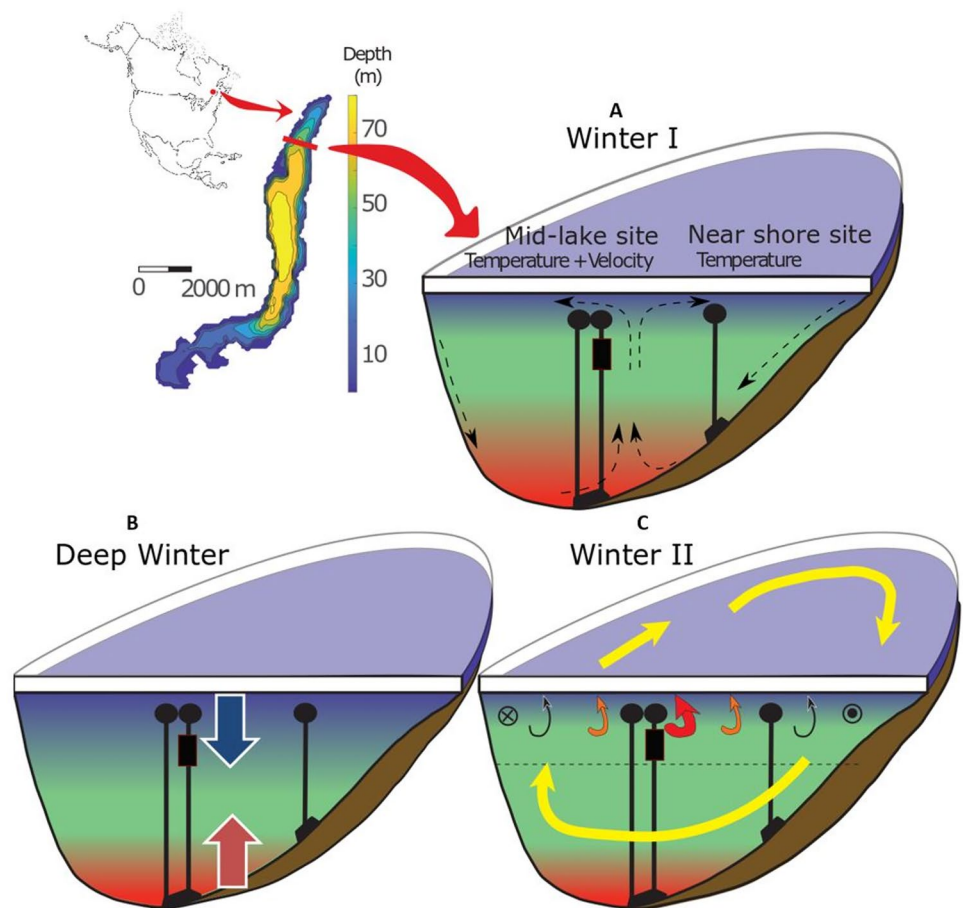
currents subsided, leading to a time period (day 44–75) of quiescent isotherms and little variability in the vertical temperature gradients (Fig. 11B), similar to the observations at Lake Sunapee (Bruesewitz et al. 2015). The sustained surface and bottom heat fluxes between 0 and 5 W/m^2 indicated that stratification stabilized, and *Deep Winter* had begun. However, the dissolved oxygen measurements during this time continued to exhibit fluctuations ±0.5 mg/L/day. On day 50–60 (Fig. 3), there was a negative slope in the surface isotherms that indicates continued ice growth. One possible explanation for the large fluctuations in dissolved oxygen is that brine rejection from ice growth in the littoral region could have produced saline density currents to the bottom of the lake, furthering internal wave action (Cortés and MacIntyre 2020). Moreover, the equilibrium conditions of *Deep Winter* could sustain wave action from *Winter I*.

As seen in Lake Sunapee in Bruesewitz et al. (2015), the characterization of *Deep winter* is most likely to occur in deep lakes, where the influence of sediment fluxes decays after initial ice freeze-up. The classification of *Deep Winter* in winter limnology is important to consider because the mechanisms governing the circulation patterns during this time are neither sediment heat flux nor radiatively driven convection, which results in this time period being highly influenced by the initial conditions of *Winter I*. Furthermore, this *Deep Winter* provides a buffer between *Winter I* and *Winter II*, as climate change continues to decrease the duration of ice cover, the presence of *Deep Winter* could disappear resulting in superimposed effects of sediment fluxes and RDC driving circulation, as would be typical in shallower lakes today.

Winter II regime

The transition from *Deep Winter* to *Winter II* was apparent on day 75, with the first observation of negative heat fluxes in the surface thermistors (Fig. 3), and an instantaneous response in the isotherms. During *Winter II,* the surface waters were heavily influenced by the thawing and refreezing of the ice surface, RDC, and ice sheet oscillations induced by wind. After RDC established a CML, the formation of a sustained density anomaly occurred in the form of a cold-water mass.

On day 75 the wind became a driving mechanism once again, with another sustained wind event of 24 m/s that likely induced ice sheet oscillations. The heterogeneity between the two moorings contributes to the hypothesis that ice sheet oscillations are once again a driving mechanism, due to the distance between the moorings. The energy from the wind event translated throughout the full depth of the water column and across the lake. The layer of vertical and horizontal flow confined to 15 m was directly correlated with

RDC and *Winter II*. When shortwave radiation was low, the flow halted (e.g., day 81–84) and it was immediately initiated again when shortwave input increased. The CML extended to 11 m on day 82 but cooled by 0.2 °C by day 84, which indicates competing forces between RDC, meltwater, and ice sheet oscillations as the dominant driving mechanism. Congruently, the sharp increase in salinity on day 83 is attributed to the collapse of the surface layer. Previously, the saline layer was supported by the temperature gradient at the ice-water interface (Forrest et al. 2013), but as RDC heated the water beneath the ice the temperature gradient no longer supported the salts accumulated at the ice-water interface, which resulted in a plunging effect of cold, saline water. The temperature profiles confirm this proposed mechanism (Fig. 6). The CML was re-established with a deepening rate, $\frac{\partial h}{\partial t} = \frac{\partial T/\partial t}{\partial T/\partial h}$, of 0.2 m/day from day 82 to 92, where $\partial T/\partial h$ was determined by taking the change in temperature from the uppermost thermistor to the thermistor at the estimated location of the CML ~11 m. The calculated deepening rate coincides with previous observations of deepening rates for RDC (e.g., Bengtsson 1996).

On day 94, another sustained wind event of 10 m/s from the west contributed to thermal heterogeneity between the mid-lake and nearshore sites. The most likely explanation for spatial heterogeneity is the response and relaxation time of ice-sheet oscillations induced by wind events. The main drivers of circulation continued to be thawing, refreezing, and wind forcing on the ice sheet until day 105. Figure 11C provides a schematic of the proposed circulation during *Winter II* as it progresses into the next phase of circulation with the possible formation of a rotating mechanism.

The evidence for a potential rotating mechanism under ice occurs from day 105 to 112 with (1) expression of a horizontally unstable, cold-water mass that persisted for 5 days in the CML; (2) increased northward and delayed positive vertical velocities, with no appreciable eastern velocities for the duration of the cold-water mass expression; (3) density gradient providing a Rossby radius less than the width of the lake; and (4) the time lag of the cold-water expression from the nearshore site to the mid-lake site. It is hypothesized that the establishment of the CML provided favorable conditions to promote a rotational feature.

The first evidence of the potential rotational feature was the expression of an unstable, cold-water mass coupled with persistent northward velocities and no appreciable eastern flow measured from the mid-lake ADCP mooring, which would indicate anticyclonic rotation. In the northern hemisphere, an anticyclonic gyre is associated with upwelling at the center (Forrest et al. 2013; Kirillin et al. 2015; Kouraev et al. 2019, 2016). Central upwelling was observed one day after the expression of the northward flow, with increased upward velocities (Fig. 7h). By assuming a

two-layer approximation, the Rossby radius reduced to ~415 m, less than the width of the sub-basin at the study site (~850 m), permitting the influence of Earth's rotation to modify the flow patterns (Forrest et al. 2013). Using the observed temperature gradient, and assuming a geostrophic balance of the rotational motion of the water mass, the theoretical azimuthal velocity, u_θ in Eq. 1, was calculated to be 0.5–0.7 cm/s.

$$f_{COR} u_\theta = \frac{\partial p}{\rho_0 \partial r} - \frac{u_\theta^2}{r}, \tag{1}$$

where f_{COR} is the Coriolis frequency at the latitude of the study site, u_θ is the azimuthal velocity, $\partial p / \partial r$ is the pressure gradient and ρ_0 is the reference density of 1000 kg/m^3. The pressure differential was calculated at the 5.5-m thermistor location between both moorings at the onset of the cold-water mass (day 105) using hydrostatic pressure and Thermal Equations of Seawater (TEOS-10) to calculate density. The distance between the two moorings, Δr, was 330 m. The Coriolis frequency at Lake Massawippi is 1.03×10^{-4} rad/s.

Furthermore, the rotational feature demonstrated the advection of a density instability (cold-water mass) that persisted for 5 days from day 108 to 113. The proposed mechanism capable of supporting this prolonged density instability is by rotation. Central upwelling or gravity currents could have produced a similar effect, but evidence (2) and (3) support a rotational feature. The cold-water mass was expressed at the depth of the convectively mixed layer, 11 m, and was first apparent at the nearshore site with a 72-h lag of expression to the mid-lake site. Using the theoretical arc length for rotational motion and theoretical azimuthal velocity, the time lag between the eastern and western mooring was approximately 72 h, which agrees with the time lag expression of the cold-water mass from the thermistor chains.

Due to the localized spatial limitations of the field deployment, the expected dome-like structure of a gyre could not be fully resolved. The rotational feature presented could be a gyre or a response to circulation patterns beyond the study site, creating a local mesoscale vortex. Expansion of the field experiment to include further extents of the lake, additional localized current measurements in the northern sub-basin, and/or a three-dimensional model would be needed to confirm the presence of a gyre at Lake Massawippi.

Ice-off regime

The transition from ice-on to ice-off was characterized by (1) significant variability between the temperature records of the nearshore and mid-lake regions; (2) expression of horizontal and vertical two-layer flows; and (3) prolonged unstable thermal stratification after complete ice-off in the interior. The absence of full mixing events at the mid-lake site for at least 28 days indicated that full mixing events after ice-off are not instantaneous. Furthermore, in the early spring, three distinct responses were observed before the onset stratification: (1) lasting effects of ice cover and spatial homogeneity period; (2) disjointed nearshore and interior processes, with multiple mixing events at the nearshore and vertical migration of a thermally unstable cold-water layer in the interior; and (3) unstable thermal stratification and spatial heterogeneity period. To our knowledge, these datasets provided the first long-term detailed analysis of the complexities of ice-off dynamics, as there is an absence of studies focusing on ice-off mixing dynamics.

Immediately following ice-off (day 114), the lake remained inversely stratified in temperature (Fig. 8). The flow structure consisted of vertically dominated fluxes from the bottom waters to the surface waters on the same order of magnitude as the horizontal fluxes. It is interesting to note that while the lake remained inversely stratified (until day 117), there appears to be flow separation with upward and downward motion initially in the upper and lower water column only to inverted at approximately day 116. Although winds were relatively high to initiate ice break-up (day 114), they were relatively low until day 117, allowing this inverse stratification to exist. The complex flow dynamics and flow separation are likely a delayed response to the ice cover breaking up and result in surface water flowing in the direction of the wind (as observed on day 115).

The second time regime consisted of multi-mixing events at or below the T_{MD} in the nearshore region and a sustained, underlying less dense cold-water layer in the pelagic region of the lake. While this is theoretically unstable, it is hypothesized that the elevated winds are promoting mixing along the boundaries of the lake which are inducing flow toward the center. It should be noted that there is a sizable negative velocity (~1 cm/s) throughout the entire water column for day 117–123. Using this as a conservative scaling of velocity over half the width of the lake (~500 m) we get a time scale of observed responses of ~14 h. The nearshore site experienced multiple instances of full vertical mixing while the mid-lake site maintained stratification for the entirety of the deployment. While the observed velocities became less pronounced as the surface waters continued to warm, this process of exchange from the nearshore downslope continued throughout. The cold-water layer was likely stabilized by the increased salt content of snowmelt that accumulated in the bottom carried by density currents (Malm 1998). Reviewing the conductivity record, which increased from ~120 to 140 μS/cm, this would increase the density from 1000.09 to 1000.11 kg/m^3, which would be enough to stabilize the water column (calculated after Pawlowicz 2008).

The absence of mixing events during this time period permitted the sustained cold-water layer to exist in the deep bottom waters. The vertical migration of the cold water created

the possibility of nutrient transport to the photic zone, which could have been the first introduction of nutrients since the fall overturn (Hampton et al. 2017). After ice-off, the bottom waters experienced large fluctuations of DO, which correlated directly with pulses of vertical flow. The DO decreased during a downward flow event (day 118–120) and upward pulses of flow (day 126–127). Then DO increased during a downward pulse of flow on day 127 and decreased again during an upward pulse of flow. The DO steadily increased during periods of no flow. The lack of correlation between the direction of the flow and increases in DO, provides further evidence of the complexity of 3D circulation. The transport of oxygenated/deoxygenated water from other locations in the lake is a likely possibility.

After day 127, nearly 13 days after the initial ice-off, the first warming of the surface waters above the temperature of maximum density began to take place and continued through the end of observations on day 142 (Fig. 9). Consistent air temperatures above freezing promoted steady warming of the surface waters and the development of stratification at both sites. When air temperatures decreased, the stratification weakened (e.g., day 129–130). The increased air temperatures and a southwesterly wind event prompted the warming of the water column to temperatures above the T_{MD}. After the warming event, the stratification began to strengthen again with consistent warming of the surface waters and deepening of the epilimnion. Additionally, the nearshore and mid-lake sites exhibited unstable thermal stratification with the hypolimnion operating below the T_{MD}, which rises to 20 m on day 137. The apparent unstable thermal stratification was likely stabilized by the salt content that accumulated in the hypolimnion. A wind-induced mixing event from day 137 to 139 resulted in temporary stable thermal stratification. The effects of this mixing event resulted in a warmer hypolimnion but still exhibited temperatures below the T_{MD}. The T_{MD}, 3.98 °C, isotherm fluctuated around 20–30 m (Fig. 10E). At this stage the water column was heavily influenced by heat fluxes, wind forcing, and salt content.

Contrary to the common thinking that ice-off is immediately followed by full vertical mixing, these observations demonstrate a much more complex dynamic that is poorly understood, as temperatures fluctuate around either side of the temperature of maximum density. This work also highlights the role that minor conductivity fluctuations have on the density stratification of the water column. The ice-off regime provides multi-mixing events that have the potential to redistribute nutrients spatially and throughout the water column. The mixing at this time period provides the first reintroduction of nutrients and dissolved oxygen to the ecosystem and could be considered more significant to the overall health of the lake than upwelling events in late spring and early fall. The dynamics during the transition

from ice-on to open water have not been adequately studied in winter limnology and present an opportunity for further field experimentation and hydrodynamic model development to extend the understanding of the linkages of physical mixing properties and the ecosystem.

Conclusions

The results presented herein for winter ice-covered temperate, mid-latitude lakes show evidence of complex circulation patterns through three distinct time periods (*Winter I*, *Deep Winter*, *Winter II*). The dominant drivers of circulation of sediment, heat flux in *Winter I* and RDC in *Winter II*, were observed to be present in Lake Massawippi; however, in this work, we identified the *Deep Winter* period using heat fluxes at the boundaries to delineate onset and duration. Immediately preceding ice-off, evidence was also found for potential rotational circulation. Finally, we were able to resolve mixing dynamics during ice-off in unprecedented detail.

Under ice, observed dynamics were initiated by sediment fluxes, radiatively driven convection, and potential formation of a rotating feature at the northern end of the lake. The transition from each winter regime was determined using heat fluxes in the surface and bottom waters. This method would be most suitable for relatively deep lakes in the mid-latitude region. Single-cell convection is the proposed dominant circulation pattern with pulses of flow initiated by sediment fluxes and suppressed by the stabilizing force of ice growth. During *Winter I*, the surface heat fluxes were > 5 W/m^2 and the bottom heat fluxes ranged from 2 to5 W/m^2. Once the heat fluxes stabilized (0–5 W/m^2 for both surface and bottom waters), the lake transitioned to an equilibrium state referred to herein as *Deep Winter*, which exhibited cyclical fluctuations in the dissolved oxygen content. The first observation of negative heat fluxes in the surface waters indicated the transition point from *Deep Winter* to *Winter II*. Then radiatively driven convection dominated the period of *Winter II*. The observed thermal structure during *Winter II* had the potential to be influenced by the Earth's rotation, fostering the formation of a rotational feature. Further research is necessary to determine the nature of rotational features and gyres under ice, such as the three-dimensional extent of gyres, interactions of circulation patterns over the full extent of the lake, initiating mechanisms for rotational circulation patterns, and temporal evolution of the rotational feature as this transport mechanism is extinguished at ice-off.

During ice-off, the extent to which the water column in a classic dimictic lake will experience full mixing was demonstrated. The water column remained below the temperature of maximum density for two weeks after ice-off and allowed for the vertical transport of a cold-water mass that was observed at both the pelagic and littoral regions of the

lake. The vertical mixing at ice-off had a direct impact on the dissolved oxygen content at the bottom of the interior of the lake. The prolonged dynamics during the transition from ice-on to ice-off presented complex mixing patterns of shear flows and potential density instabilities challenging the conventional conceptual model of very quick turnover and requires further investigation to determine the impact of these events on water quality, distribution of nutrients, dissolved oxygen, and/or pollutants. In addition, mixing at ice-off should be evaluated with potential climate scenarios to understand the variability in this dynamic period. Further field experiments with increased spatial resolution of temperature and dissolved oxygen are needed to determine the three-dimensional circulation patterns and the subsequent impact on dissolved oxygen during the ice-covered season and process of ice-off.

Declarations

References

Austin J (2019) Observations of radiatively driven convection in a deep lake. Limnol Oceanogr. https://doi.org/10.1002/lno.11175

Beletsky DV (1996) Numerical modelling of large-scale circulation in Lakes Onega and Ladoga. Hydrobiologia 322(1–3):75–80. https://doi.org/10.1007/BF00031808

Beletsky D, Saylor JH, Schwab DJ (1999) Mean circulation in the Great Lakes. J Great Lakes Res 25(1):78–93. https://doi.org/10.1016/S0380-1330(99)70718-5

Bendat JS, Piersol AG (1986) Random data: analysis and measurement procedures, 2nd edn. Wiley

Bengtsson L (1996) Mixing in ice-covered lakes. Hydrobiologia 322(1–3):91–97. https://doi.org/10.1007/BF00031811

Bouffard D, Boegman L (2012). Basin-Scale Internal Waves. https://doi.org/10.1007/978-1-4020-4410-6

Bouffard D, Zdorovennov RE, Zdorovennova GE, Pasche N, Wüest A, Terzhevik AY (2016) Ice-covered Lake Onega: effects of radiation on convection and internal waves. Hydrobiologia 780(1):21–36. https://doi.org/10.1007/s10750-016-2915-3

Bruesewitz DA, Carey CC, Richardson DC, Weathers KC (2015) Under-ice thermal stratification dynamics of a large, deep lake revealed by high-frequency data. Limnol Oceanogr 60:347–359. https://doi.org/10.1002/lno.10014

Cavaliere E, Baulch HM (2020) Winter in two phases: Long-term study of a shallow reservoir in winter. Limnol Oceanogr 66:1335–1352. https://doi.org/10.1002/lno.11687

Cortés A, MacIntyre S (2020) Mixing processes in small arctic lakes during spring. Limnol Oceanogr 65(2):260–288. https://doi.org/10.1002/lno.11296

Farmer DM (1975) Penetrative convection in the absence of mean shear. Q J R Meteorol Soc 101(430):869–891. https://doi.org/10.1002/qj.49710143011

Forrest AL, Pieter R, Lim DSS (2008) Convectively driven transport in temperate lakes. Limnol Oceanogr 53(5, Part 2):2321–2332

Forrest AL, Laval BE, Pieters R, Lim DSS (2013) A cyclonic gyre in an ice-covered lake. Limnol Oceanogr 58(1):363–375

Ghane A, Boegman L (2021) Turnover in a small Canadian shield lake. Limnol Oceanogr 66:3356–3373. https://doi.org/10.1002/lno.11884

Hampton SE, Galloway AWE, Powers SM, Ozersky T, Woo KH, Batt RD, Labou SG, O'Reilly CM, Sharma S, Lottig NR, Stanley EH, North RL, Stockwell JD, Adrian R, Weyhenmeyer GA, Arvola L, Baulch HM, Bertani I, Bowman LL, Carey CC, Catalan J, Colom-Montero W, Domine LM, Felip M, Corinna G, Grossart HP, Haberman J, Haldna M, Hayden B, Higgins SN, Jolley JC, Kahilainen KK, Kaup E, Kehoe MJ, MacIntyre S, Mackay AW, Mariash HL, McKay RM, Nixdorf B, Nõges P, Nõges T, Palmer M, Pierson DC, Post DM, Pruett MJ, Rautio M, Read JS, Roberts SL, Rücker J, Sadro S, Silow EA, Smith DE, Sterner RW, Swann GEA, Timofeyev MA, Toro M, Twiss MR, Vogt RJ, Watson SB, Whiteford EJ, Xenopoulos MA (2017) Ecology under lake ice. Ecol Lett 20(1):98–111. https://doi.org/10.1111/ele.12699

Huttula T, Pulkkanen M, Arkhipov B, Leppäranta M, Solbakov V, Shirasawa K, Salonen K (2010) Modelling circulation in an ice-covered lake. Estonian J Earth Sci 59(4):298–309. https://doi.org/10.3176/earth.2010.4.06

Jonas T, Terzhevik AY, Mironov DV, Wüest A (2003) Radiatively driven convection in an ice-covered lake investigated by using temperature microstructure technique. J Geophys Res C Oceans 108(6):14–21. https://doi.org/10.1029/2002JC001316

Kerfoot WC, Budd JW, Green SA, Cotner JB, Biddanda BA, Schwab DJ, Vanderploeg HA (2008) Doughnut in the desert: Late-winter production pulse in southern Lake Michigan. Limnol Oceanogr 53(2):589–604. https://doi.org/10.4319/lo.2008.53.2.0589

Kirillin G, Leppäranta M, Terzhevik A, Granin N, Bernhardt J, Engelhardt C, Zdorovennov R (2012) Physics of seasonally ice-covered lakes: a review. Aquat Sci 74(4):659–682. https://doi.org/10.1007/s00027-012-0279-y

Kirillin GB, Forrest AL, Graves KE, Fischer A, Engelhardt C, Laval BE (2015) Axisymmetric circulation driven by marginal heating in ice-covered lakes. Geophys Res Lett 42(8):2893–2900. https://doi.org/10.1002/2014GL062180

Kouraev AV, Zakharova EA, Rémy F, Kostianoy AG, Shimaraev MN, Hall NMJ, Suknev YaA (2016) Giant ice rings on lakes Baikal and Hovsgol: Inventory, associated water structure and potential

formation mechanism. Limnol Oceanogr 61(3):1001–1014. https://doi.org/10.1002/lno.10268

Kouraev AV, Zakharova EA, Rémy F, Kostianoy AG, Shimaraev MN, Hall NMJ, Suknev AY (2019) Giant ice rings on lakes and field observations of lens-like eddies in the Middle Baikal (2016–2017). Limnol Oceanogr 64(6):2738–2754. https://doi.org/10.1002/lno.11338

Kundu PK, Cohen IM, Dowling DR (2016) Fluid mechanics, 6th edn. Academic Press, Oxford

Likens GE, Ragotzkie RA (1965) Vertical water motions in a small ice-covered lake. J Geophys Res 70(10):2333–2344

MacIntyre S, Cortés A, Sadro S (2018) Sediment respiration drives circulation and production of CO_2 in ice-covered Alaskan artic lakes. Limnol Oceanogr Lett. https://doi.org/10.1002/lol2.10083

Malm J (1998) Bottom buoyancy layer in an ice-covered lake. Water Resour Res 34(11):2981–2993. https://doi.org/10.1029/98WR01904

Malm J, Terzhevik A, Bengtsson L, Boyarinov P, Glinsky A, Palshin N, Petrov M (1997) Temperature and salt content regimes in three shallow ice-covered lakes: 1. Temperature, salt content, and density structure. Nord Hydrol 28(2):99–128. https://doi.org/10.2166/nh.1997.0007

Mironov D, Terzhevik A, Kirillin G, Jonas T, Malm J, Farmer D (2002) Radiatively driven convection in ice-covered lakes: Observations scaling and a mixed layer model. J Geophys Res Oceans 107(C4). https://doi.org/10.1029/2001JC000892

Olsthoorn J, Tedford EW, Lawrence GA (2022) Salt-fingering in seasonally ice-covered lakes. Geophys Rese Lett. https://doi.org/10.1029/2022GL097935

Pawlowicz R (2008) Calculating the conductivity of natural waters. Limnolo Oceanogr Methods 6(9):489–501. https://doi.org/10.4319/lom.2008.6.489

Perga M, Minaudo C, Doda T, Arthaud F, Beria H, Chmiel HE, Escoffier N, Lambert T, Napolleoni R, Obrador B, Perolo P, Ruegg J, Ulloa H, Bouffard D (2023) Near-bed stratification controls bottom hypoxia in ice-covered alpine lakes. Limnol Oceanogr 9999:1–15. https://doi.org/10.1002/lno.12341

Rahm L (1985) The thermally forced circulation in a small, ice-covered lake. Limnol Oceanogr 30(5):1122–1128. https://doi.org/10.4319/lo.1985.30.5.1122

Ramón CL, Ulloa HN, Doda T, Winters KB, Bouffard D (2021) Bathymetry and latitude modify lake warming under ice. Hydrol Earth Syst Sci 25:1813–1825. https://doi.org/10.5194/hess-25-1813-2021

Rizk W, Kirillin G, Leppa M (2014) Basin-Scale Circulation and Heat Fluxes in Ice-Covered Lakes 59(2):445–464. https://doi.org/10.4319/lo.2014.59.02.0445

Salonen K, Pulkkanen M, Salmi P, Griffiths RW (2014) Interannual variability of circulation under spring ice in a boreal lake. Limnol Oceanogr 59(6):2121–2132. https://doi.org/10.4319/lo.2014.59.6.2121

Steel HCB, McKay CP, Andersen DT (2015) Modeling circulation and seasonal fluctuations in perennially ice-covered and ice-walled lake Untersee, Antarctica. Limnol Oceanogr 60(4):1139–1155. https://doi.org/10.1002/lno.10086

Ulloa HN, Winters KB, Wüest A, Bouffard D (2019) Differential heating drives downslope flows that accelerate mixed-layer warming in ice-covered waters. Geophys Res Lett 46(23):13872–13882. https://doi.org/10.1029/2019GL085258

Vehmaa A, Salonen K (2009) Development of phytoplankton in Lake Pääjärvi (Finland) during under-ice convective mixing period. Aquat Ecol 43(3):693–705. https://doi.org/10.1007/s10452-009-9273-4

Yang B, Wells MG, Li J, Young J (2020) Mixing, stratification, and plankton under lake-ice during winter in a large lake: Implications for spring dissolved oxygen levels. Limonology and Oceanography 64:2713–2729. https://doi.org/10.1002/lno.11543

Yang B et al (2021) A new thermal categorization of ice-covered lakes. Geophys Res Lett. https://doi.org/10.1029/2020GL091374

Zdorovennova GE (2009) Spatial and temporal variations of the water-sediment thermal structure in shallow ice-covered lake Vendyurskoe (Northwestern Russia). Aquat Ecol 43(3):629–639. https://doi.org/10.1007/s10452-009-9277-0